

Characterization of Nanoparticles by Solvent Infrared Spectroscopy

Johannes Kiefer,^{*†‡§} Janet Grabow,^{||} Heinz-Dieter Kurland,^{||} and Frank A. Müller^{||}

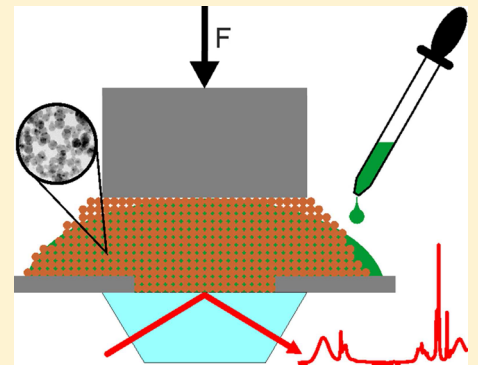
[†]Technische Thermodynamik, Universität Bremen, Badgasteiner Str. 1, 28359 Bremen, Germany

^{||}Otto Schott Institute of Materials Research (OSIM), Friedrich Schiller University Jena, Jena, Germany

[‡]School of Engineering, University of Aberdeen, Aberdeen, United Kingdom

[§]Erlangen Graduate School in Advanced Optical Technologies, Universität Erlangen-Nürnberg, Erlangen, Germany

ABSTRACT: The characterization of the surface chemistry of nanoparticles using infrared spectroscopy of adsorbed solvents is proposed. In conventional IR spectroscopy of nanomaterials the capability of characterizing the chemistry of the surface is limited. To overcome these limitations, we record IR spectra of different solvents inside a fixed bed of the nanopowder to be tested. Using water and different alcohols as solvents enables the characterization of the nanomaterial's surface chemistry via the molecular interactions affecting the hydrogen-bonding network in the solvent. Different ceramic nanopowders (titania, two different iron oxides, and iron oxide nanocrystallites embedded in a closed silica matrix) are studied using water, ethanol, and *n*-butanol as solvents. The OH stretching region of the IR spectra reveals characteristic differences in the surface chemistry of the nanoparticles. The proposed method is fast and straightforward, and hence, it can be a versatile tool for rapid screening.



Nanotechnology experiences an ever-increasing interest in academia and industry. Nanoscale substances are not only functional materials with desirable properties, they also facilitate the development of new technologies and compact devices. Areas of application range from the medical and pharmaceutical sector^{1,2} to electronics,^{3,4} catalysis,^{5,6} and chemical sensing.^{7,8}

The key part of a nanomaterial determining its properties is the surface. It represents the interface between a particle and its environment, and it determines how the two communicate and influence each other. Consequently, there is a need for characterizing the surface structure and chemistry of nanomaterials. In principle, there are many established methods for surface characterization of nanostructured materials. For example, the morphology and size can be studied using electron microscopy techniques^{9–11} and atomic force microscopy (AFM).^{12–14} The surface chemistry, however, is more difficult to probe. Suitable methods include second-order nonlinear optical techniques such as second harmonic generation (SHG) and sum-frequency generation (SFG).^{15,16} Besides their nonintrusive nature, the benefit of these methods is that the signal is explicitly generated at the surface, not biased from bulk contributions. However, the experimental complexity and costs are disadvantages. Further spectroscopic approaches include Auger electron spectroscopy (AES), X-ray photoelectron spectroscopy (XPS), and low energy ion scattering (LEIS).^{17,18}

As an alternative, it would be beneficial to use standard equipment available in most analytical laboratories, anyway, for studying the surface chemistry of a nanomaterial. Infrared (IR) spectroscopy is such a method. However, neither in transmission mode nor in attenuated total reflection (ATR)

configuration does it provide sufficient spatial resolution. Hence, the signal will be governed by contributions from bulk material rather than the surface. Nevertheless, IR spectroscopy has been successfully applied to study nanomaterials and surface effects. For example, it can be used to identify functional groups on the surface of functionalized nanoparticles.¹⁹ It was also employed to study the physisorption of molecules at the surface of nanomaterials.^{20,21} Furthermore, IR spectra of suspensions were used to extract information about specific surface area, surface charge density, and concentration of a nanomaterial.^{22–24} These studies, however, focused on the characterization of specific systems, namely, the combination of a nanomaterial and a surrounding medium. In the following, we make a step toward using IR spectroscopy in a more general way for the investigation of chemical properties of the surface of nanomaterials.

In this article, we demonstrate the application of an indirect means of characterizing the surface chemistry of nanomaterials via the infrared spectroscopic analysis of their molecular environment. For this purpose, the nanomaterial is put in contact with different solvents. Selecting solvents with systematically varied chemical properties allows not only distinguishing between different types of nanoparticles, it also provides a useful image of their surface chemistry. Zobel et al. have shown recently that different solvent molecules form a rather similar and relatively small solvation shell around colloidal nanoparticles.²⁵ However, the perturbation of the

Received: September 24, 2015

Accepted: November 22, 2015

Published: November 23, 2015

hydrogen-bonding network in the solvent can go significantly beyond this distance so that a large fraction of the solvent molecules is affected and show a modified vibrational signature.²⁶

■ EXPERIMENTAL SECTION

In order to make the most of this effect, a fixed bed of the powdery nanomaterial to be tested is prepared on the internal reflection element (IRE) of an attenuated total reflection (ATR) Fourier-transform infrared (FTIR) spectrometer, as illustrated in Figure 1. Note that the IRE is often referred to as

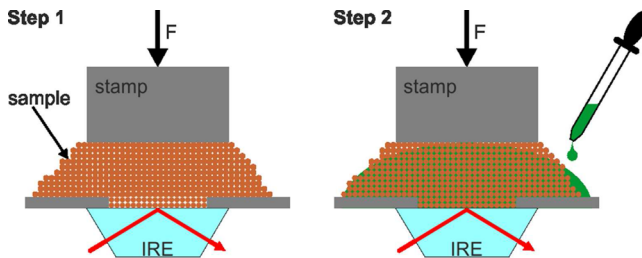


Figure 1. Illustration of the experimental procedure. In step 1, the nanopowder sample is fixed between the ATR stamp and the IRE applying a moderate force F . In step 2, the solvent is added to fill the pores.

ATR crystal or IR crystal. The pores in the fixed powder bed are then filled with a solvent. Resulting molecular interactions with the nanoparticles' surfaces affect the vibrational structure of the solvent. Performing a series of measurements with systematically varied solvents allows the analysis of the surface chemistry of the nanomaterial. As an example, we chose water, ethanol, and butanol as solvents representing liquids with differently balanced polar and nonpolar moieties. Deionized water was prepared with a resistivity of 18 M Ω ·cm by a purification system. Ethanol and *n*-butanol with purity >99% were purchased from Fisher Scientific and used as received.

The measurements were carried out on a Bruker Vertex v70 FTIR spectrometer equipped with a diamond ATR accessory. The number of reflections at the surface is 1, and the reflection angle is 45°. Spectra were recorded taking 16 scans with a nominal resolution of 1 cm⁻¹. Four exemplary nanopowders representing a range of functional ceramic materials were tested: (i) a photocatalytically active anatase (TiO_2) nanopowder, (ii) a ferrimagnetic maghemite ($\gamma\text{-}Fe_2O_3$) nanopowder, (iii) a nanopowder mixture consisting of $\gamma\text{-}Fe_2O_3$ (53 mass%) and $\epsilon\text{-}Fe_2O_3$ (47 mass%) nanoparticles combining high saturation magnetization and high magnetic coercivity, and (iv) superparamagnetic hybrid nanoparticles comprising $\gamma\text{-}Fe_2O_3$ nanocrystallites embedded in a closed spherical matrix of amorphous silica ((am) SiO_2). These powders were prepared using the CO₂ laser vaporization (LAVA) method.²⁷ In brief, coarse-grained ceramic raw powders or raw powder mixtures, respectively, were vaporized in the intense focus of the beam from a continuous-wave CO₂ laser at ambient pressure. Subsequent rapid cooling in the process gas induces a fast condensation of the vapor resulting in the formation of single phase or hybrid nanoparticles. The TiO_2 nanopowder²⁸ (in the following, the sample is referred to as "anatase") was prepared starting from an anatase raw powder, the $\gamma\text{-}Fe_2O_3$ nanopowder²⁹ (sample " $\gamma\text{-}Fe_2O_3$ ") and the $\gamma\text{-}Fe_2O_3/\epsilon\text{-}Fe_2O_3$ nanopowder mixture²⁹ (sample " $\gamma/\epsilon\text{-}Fe_2O_3$ ") from a hematite raw powder ($\alpha\text{-}Fe_2O_3$) raw powder condensed in argon and air,

respectively, and the $\gamma\text{-}Fe_2O_3@(am)SiO_2$ hybrid nanoparticles³⁰ (sample "SiliFe") from a mixture of a hematite raw powder (33 mass%) with quartz sand (67 mass%). Representative transmission electron micrographs of each nanopowder sample are shown in Figure 2.

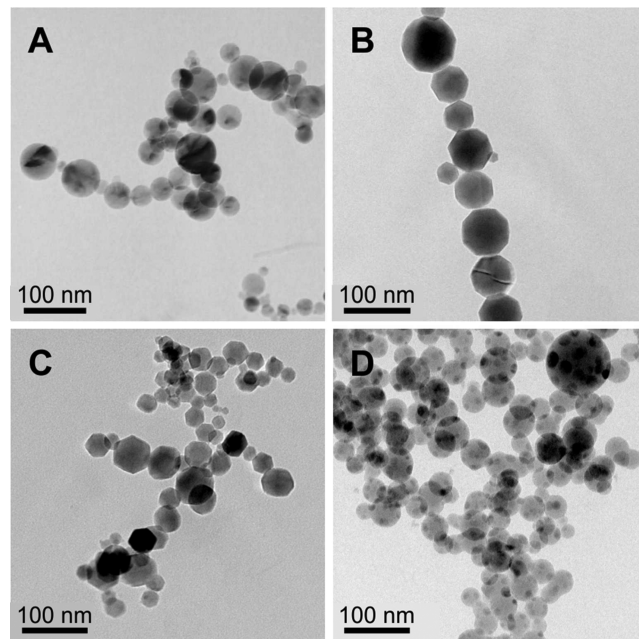


Figure 2. Transmission electron micrographs of the four nanopowder samples under investigation: (A) anatase nanoparticles, (B) $\gamma\text{-}Fe_2O_3$ nanoparticles, (C) $\gamma/\epsilon\text{-}Fe_2O_3$ nanoparticles, and (D) SiliFe nanoparticles.

Prior to an experiment, a small amount of the nanopowder was put on the IRE and fixed with the metal stamp of the instrument. Thus, a fixed bed of nanoparticles was created on top of the IRE. The measurement area on the IRE was a spot of ~1.5 mm diameter.³¹ This spot is sufficiently large to ensure that the sample is statistically representative in terms of size distribution, shape, and orientation of the nanoparticles. In the second step, a small droplet of solvent was added with a pipet in order to wet the particles and the IRE surface. Then the spectrum was recorded. The reproducibility of this procedure was checked by analyzing every combination of solvent and nanomaterial ten times with a freshly prepared sample. Varying the amounts of powder and solvent did not change the spectrum. This shows that the preparation of the fixed bed compressed with the stamp and the subsequent wetting leads to a reproducible sample at the IRE surface enabling the interaction with the evanescent field of the reflected IR radiation. The major part of the IRE surface appears to be in contact with the solvent, because distinct spectral features originating directly from the nanoparticles could not be observed in the presence of the solvent.

■ RESULTS AND DISCUSSION

The part of the spectrum most sensitive to changes in the molecular environment is the OH stretching region, as it is directly affected whenever the hydrogen-bonding network of any of the solvents used here is altered. Hence, we focus on this region in our analysis. Figure 3 illustrates the OH stretching region of the spectra recorded with water. The spectra in panel

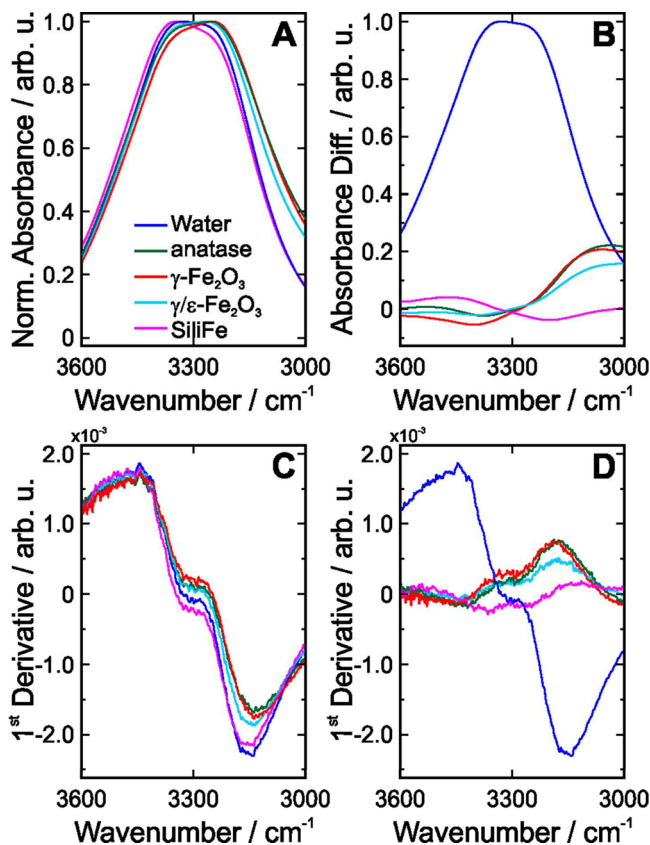


Figure 3. IR spectra of the OH stretching band of pure water and the four nanopowder samples as well as the derived data: (A) normalized spectra, (B) difference spectra, (C) first derivative spectra of normalized spectra, (D) first derivative spectra of difference spectra. In B, the normalized water spectrum is shown for comparison. In D, the first derivative spectrum of the normalized water spectrum is shown for comparison.

A are normalized with respect to the maximum value in the range displayed. This allows an improved comparison of the band shapes. For a detailed analysis, the OH stretching band is often deconvolved into individual peaks representing different interaction states of water molecules.^{32,33} As an estimate, the signals at frequencies above 3300 cm^{-1} can be assigned to those molecules that are only weakly involved in hydrogen-bonding interactions. The signals at lower frequencies are attributed to strongly hydrogen-bonded water molecules. An analogue interpretation can be applied to the ethanol and butanol spectra shown in Figures 4 and 5, respectively. In order to emphasize the changes in the spectra due to the presence of nanoparticles, the panels B display the difference spectra. Moreover, the panels C and D show the derivative spectra corresponding to panels A and B, respectively.

The data in Figures 3–5 show distinct differences for the different nanoparticles. As the solvents water, ethanol, and butanol exhibit systematically varying dielectric constants (80, 24.5, and 18, respectively) because of their joint hydroxyl group and the remaining group with decreasing polarity. Hence, they can interact with the nanoparticle surface via different mechanisms such as hydrogen-bonding, polar interactions, and van der Waals forces. Here, we focus on the hydrogen-bonding interactions, and hence, in Figures 3–5, the OH stretching bands are displayed. This is sufficient in all cases

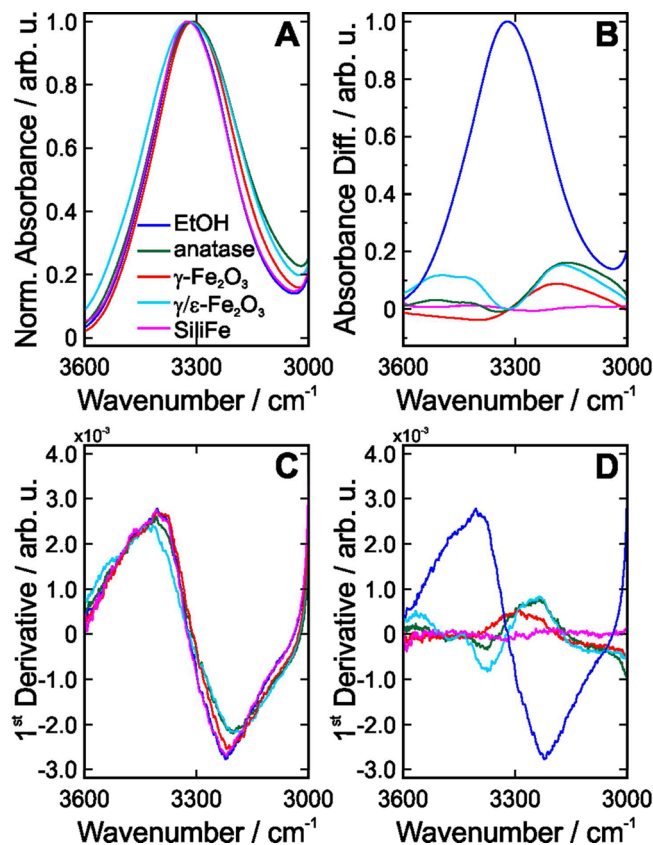


Figure 4. IR spectra of the OH stretching band of pure ethanol and the four nanopowder samples as well as the derived data: (A) normalized spectra, (B) difference spectra, (C) first derivative spectra of normalized spectra, (D) first derivative spectra of difference spectra. In B, the normalized ethanol spectrum is shown for comparison. In D, the first derivative spectrum of the normalized ethanol spectrum is shown for comparison.

considered here, as the OH band is highly sensitive to changes in the hydrogen-bonding network.

The results can be summarized and compared in a rather qualitative manner. For this purpose, Table 1 considers the behavior of the high and low wavenumber wings of the OH stretching bands by assigning “++” and “+” to strong and moderate enhancement, respectively, “—” and “−” to strong and moderate attenuation, respectively, and “o” whenever no significant change is observed. In water, the spectral regions referred to as high and low wavenumber wings are assigned to the regions above and below 3300 cm^{-1} , respectively. In the ethanol and butanol spectra, the distinction between the high and low wavenumber wings is made with respect to the absorbance maximum in the spectrum of the pure solvent. Changes of less than 2.5% were classified as “o”, changes between 2.5% and 10% were classified as “+” or “−”, and changes exceeding 10% were classified as “++” or “—”. From Table 1 it is obvious that each type of nanopowder exhibits a unique combination of markers characterizing its effects on the hydrogen-bonding network of the respective solvents. Further data analysis using more sophisticated methods such as a mathematical deconvolution of the spectra may provide further information, but this is beyond the scope of the present work.

The anatase particles show a significant enhancement of the low frequency wing for each solvent. This spectral region is characteristic of those solvent molecules, which are strongly

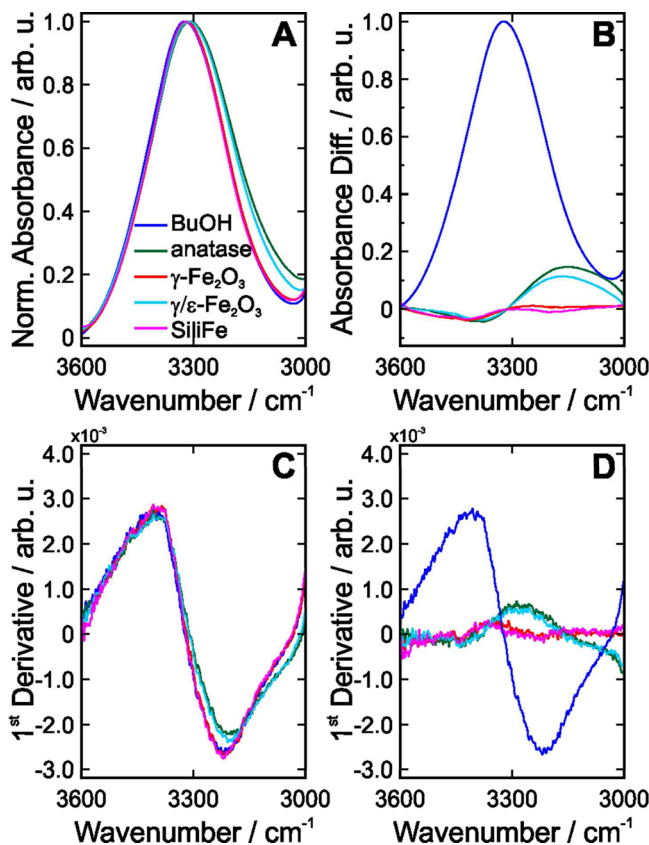


Figure 5. IR spectra of the OH stretching band of pure butanol and the four nanopowder samples as well as the derived data: (A) normalized spectra, (B) difference spectra, (C) first derivative spectra of normalized spectra, (D) first derivative spectra of difference spectra. In B, the normalized butanol spectrum is shown for comparison. In D, the first derivative spectrum of the normalized butanol spectrum is shown for comparison.

involved in hydrogen bonding. Hence, it can be concluded that the presence of TiO₂ strengthens the hydrogen-bonding network. On the high frequency wing, the OH band of water shows virtually no change, while ethanol and butanol reveal a moderate enhancement and attenuation, respectively. This means that the fraction of weakly hydrogen-bonded ethanol molecules increases, while the corresponding fraction in butanol decreases upon nanoparticle addition. The titania nanoparticles were obtained as anatase,²⁸ and the interactions of this modification with liquid water have been studied in a few articles. Tikanen et al.³⁴ developed a method for determining the anatase concentration from IR spectra of aqueous suspensions taking into consideration the changes of the refractive index and the absorption index. This is important

when quantitative information needs to be gained. In the present case, however, a qualitative assessment is sufficient and thus, such effects are not taken into account. Takeuchi et al.³⁵ studied the structure of water clusters adsorbed on titania surfaces. They concluded that the water molecules are stabilized upon adsorption on the TiO₂ surface via strong hydrogen-bonding evidenced by the red-shift of the spectral bands. The proposed model explains the behavior by chemisorption of a water monolayer at which further molecules are physisorbed. The observed red-shift of the OH stretching band manifests in the normalized spectrum in Figure 3A as a signal increase of the low frequency wing while the high frequency wing remains virtually constant. Chemically, the titania particles can be considered as surface with alternating Ti and O ions. The water molecules interact via their oxygen atom with the titanium ions. It is also possible that oxygen ions at the titania surface are protonated, thus, enabling the formation of hydrogen-bonds with water molecules.³⁵ In the alcohol cases, the potential photocatalytical activity of TiO₂ has to be taken into account. As discussed by Shepot'ko and Davydov³⁶ and Glisenti,³⁷ alcohols can adsorb to the titania surface and be catalytically converted, decomposed, and oxidized under certain temperature and pressure conditions. In the present work, the measurements were carried out at room temperature and pressure, and illumination of the samples with UV light was avoided. Therefore, such catalytic effects were not observed.

Intuitively, the two iron oxide nanopowders γ-Fe₂O₃ and γ/ε-Fe₂O₃ would appear to have very low potential to be distinguished with the proposed method. However, from a look at the spectra in Figures 3–5 and inspecting Table 1, it is obvious that they do exhibit differences in their interactions with the solvents. γ-Fe₂O₃ has a crystalline structure, and hence, the solvent molecules may arrange themselves in a fairly regular manner at the surface like in the anatase case discussed above. The spectroscopic differences between γ-Fe₂O₃ and γ/ε-Fe₂O₃ are so significant that it is likely that the polymorph ε-Fe₂O₃ nanoparticles in the mixture dominate the interactions with the solvents. In particular, in ethanol, large differences in the behavior of OH stretching modes can be found. While there is a moderate decrease of the high wavenumber wing for γ-Fe₂O₃, there is a strong increase in the γ/ε-Fe₂O₃ case. This indicates that the fraction of weakly hydrogen-bonded ethanol molecules increases in the presence of the γ/ε-Fe₂O₃ nanopowder. Interestingly, the low wavenumber wing increases moderately and strongly for γ-Fe₂O₃ and γ/ε-Fe₂O₃, respectively. This suggests that the hydrogen-bonding between the already strongly hydrogen-bonded molecules is further enhanced. Both effects together lead to a significant broadening of the OH stretching band in the presence of γ/ε-Fe₂O₃ nanoparticles.

The last nanomaterial, SiliFe, consists of γ-Fe₂O₃ embedded in a spherical silica matrix. The spectral appearance of the OH

Table 1. Qualitative Comparison of the Nanoparticle Influence on the Solvent OH Stretching Band^a

nanoparticle	anatase		γ-Fe ₂ O ₃		γ/ε-Fe ₂ O ₃		SiliFe	
solvent	high ν	low ν	high ν	low ν	high ν	low ν	high ν	low ν
water	o	++	—	++	o	++	+	—
ethanol	+	++	—	+	++	++	o	o
butanol	—	++	—	o	—	++	—	o

^aIn water, the spectral regions referred to as high and low wavenumber wing are assigned to the regions above and below 3300 cm⁻¹, respectively. In the ethanol and butanol spectra, the distinction between the high and low wavenumber wings is made with respect to the absorbance maximum in the spectrum of the pure solvent.

bands reassure the previous findings that the entire particle surface consists of silica.³⁰ There are virtually no similarities with the pure $\gamma\text{-Fe}_2\text{O}_3$ case in water and ethanol. Due to the gas-phase synthesis of the particles in the LAVA process, it is reasonable to assume that the surface does initially not exhibit any hydroxyl groups. Upon water addition, hydroxylation is very likely though, which leads to a very different appearance of the OH stretching band in Figure 3. The high wavenumber wing of the band increases, while the low wavenumber wing decreases. This indicates that the water hydrogen-bonding network is significantly weakened in the presence of the nanoparticles. One possible chemisorption mechanism is that a water molecule interacts with a Si—O—Si site, resulting in two Si—OH groups. Due to the reduced polarity of the Si bound hydroxyl group compared to water, the hydrogen-bonding ability is reduced and, hence, a weakened hydrogen-bonding network manifests in the vicinity of the particles. Another possible explanation of the behavior could be that the chemisorption of the inner hydration shell leads to the dissociation of water molecules and a charge separation. As a consequence, significant polar interactions may lead to a reduction of the hydrogen-bonding. The first chemisorption mechanism appears more likely, and it is also in agreement with the literature.³⁸ The fact that the ethanol and butanol OH bands do virtually not change in the presence of the SiliFe nanoparticles provides further support for the hypothesis of a dissociative chemisorption of water molecules. If it was a pure hydrogen-bonding mechanism at the silica surface, the alcohols should experience a weaker but similar effect.

CONCLUSION

In conclusion, we have shown that solvent infrared spectroscopy (SIRS) is a useful method for characterizing the surface chemistry of nanoparticles. Employing a range of solvents with systematically varied polar and nonpolar functional groups allows a detailed assessment of the effects the nanoparticles impose on their molecular environment. The method is simple and reproducible, and thus, it has a high potential to become an established approach in the list of methods frequently used for the characterization of nanoparticles.

In the nanomaterial–solvent combinations tested here, butanol turns out to be the least specific solvent. However, it must be kept in mind that the oxide nanomaterials studied here are supposed to form hydrogen-bonds and even allow chemisorption. Looking at nonpolar materials such as polymers and carbonaceous materials may be a different story and reveal the usefulness of employing solvents with significant nonpolar moieties.

The present work focused on distinguishing different types of nanomaterials in terms of their surface chemistry. Future work will investigate the effects of different particle sizes and shapes of the same chemical compound.

AUTHOR INFORMATION

Corresponding Author

*E-mail: kiefer@uni-bremen.de.

Notes

The authors declare no competing financial interest.

ACKNOWLEDGMENTS

Part of this work was supported by EPSRC (Grant EP/K00090X/1).

REFERENCES

- (1) Mattei, T. A.; Rehman, A. A. *Neurosurg. Rev.* **2015**, *38*, 27.
- (2) Qasim, M.; Lim, D. J.; Park, H.; Na, D. *J. Nanosci. Nanotechnol.* **2014**, *14*, 7374.
- (3) Subramanian, V.; Lee, T. *Nanotechnology* **2012**, *23*, 340201.
- (4) Goodnick, S.; Korkin, A.; Krstic, P.; Mascher, P.; Preston, J.; Zaslavsky, A. *Nanotechnology* **2010**, *21*, 130201.
- (5) Jin, R. *Nanotechnol. Rev.* **2012**, *1*, 31.
- (6) Daniel, M. C.; Astruc, D. *Chem. Rev.* **2004**, *104*, 293.
- (7) Sharma, S.; Madou, M. *Philos. Trans. R. Soc., A* **2012**, *370*, 2448.
- (8) Koedrith, P.; Thasiphu, T.; Tuitemwong, K.; Boonprasert, R.; Tuitemwong, P. *Sensors Mater.* **2014**, *26*, 711.
- (9) Liu, J. Y. *J. Electron Microsc.* **2005**, *54*, 251.
- (10) Su, D. S.; Zhang, B. S.; Schlögl, R. *Chem. Rev.* **2015**, *115*, 2818.
- (11) Zhang, B. S.; Su, D. S. *Small* **2014**, *10*, 222.
- (12) Jiang, P.; Xie, S. S.; Pang, S. J.; Gao, H. *J. Appl. Surf. Sci.* **2002**, *191*, 240.
- (13) Mechler, A.; Kopniczky, J.; Kokavec, J.; Hoel, A.; Granqvist, C. G.; Heszler, P. *Phys. Rev. B: Condens. Matter Mater. Phys.* **2005**, *72*, 125407.
- (14) Ebenstein, Y.; Nahum, E.; Banin, U. *Nano Lett.* **2002**, *2*, 945.
- (15) Schneider, L.; Peukert, W. *Part. Part. Syst. Charact.* **2006**, *23*, 351.
- (16) Geiger, F. M. *Annu. Rev. Phys. Chem.* **2009**, *60*, 61.
- (17) Baer, D. R.; Gaspar, D. J.; Nachimuthu, P.; Techane, S. D.; Castner, D. G. *Anal. Bioanal. Chem.* **2010**, *396*, 983.
- (18) Baer, D. R.; Engelhard, M. H.; Johnson, G. E.; Laskin, J.; Lai, J.; Mueller, K.; Munusamy, P.; Thevuthasan, S.; Wang, H.; Washton, N.; Elder, A.; Baisch, B. L.; Karakoti, A.; Kuchibhatla, S. V. N. T.; Moon, D. *J. Vac. Sci. Technol., A* **2013**, *31*, 050820.
- (19) Zhang, B.; Yan, B. *Anal. Bioanal. Chem.* **2010**, *396*, 973.
- (20) Mudunkotuwa, I. A.; Al Minshid, A.; Grassian, V. H. *Analyst* **2014**, *139*, 870.
- (21) Griffiths, D. M.; Marshall, K.; Rochester, C. H. *J. Chem. Soc., Faraday Trans. 1* **1974**, *70*, 400.
- (22) Wittmar, A.; Ulbricht, M. *Ind. Eng. Chem. Res.* **2012**, *51*, 8425.
- (23) Tickanen, L. D.; Tejedor-Tejedor, M. I.; Anderson, M. A. *Langmuir* **1997**, *13*, 4829.
- (24) Lagström, T.; Gmür, T. A.; Quaroni, L.; Goel, A.; Brown, M. A. *Langmuir* **2015**, *31*, 3621.
- (25) Zobel, M.; Neder, R. B.; Kimber, S. A. *J. Science* **2015**, *347*, 292.
- (26) Kiefer, J.; Toni, F.; Wirth, K.-E. *J. Raman Spectrosc.* **2015**, *46*, 1124.
- (27) Kurland, H.-D.; Grabow, J.; Müller, F. A. *J. Eur. Ceram. Soc.* **2011**, *31*, 2559.
- (28) Kurland, H.-D.; Stötzl, C.; Grabow, J.; Zink, I.; Müller, E.; Staupendahl, G.; Müller, F. A. *J. Am. Ceram. Soc.* **2010**, *95*, 1282.
- (29) Stötzl, C.; Kurland, H.-D.; Grabow, J.; Dutz, S.; Müller, E.; Sierka, M.; Müller, F. A. *Cryst. Growth Des.* **2013**, *13*, 4868.
- (30) Stötzl, C.; Kurland, H.-D.; Grabow, J.; Müller, F. A. *Nanoscale* **2015**, *7*, 7734.
- (31) Kiefer, J.; Rasul, N. H.; Ghosh, P. K.; Von Lieres, E. *J. Membr. Sci.* **2014**, *452*, 152.
- (32) Schmidt, D. A.; Miki, K. *J. Phys. Chem. A* **2007**, *111*, 10119.
- (33) Kiefer, J.; Frank, K.; Schuchmann, H. P. *Appl. Spectrosc.* **2011**, *65*, 1024.
- (34) Tickanen, L. D.; Tejedor-Tejedor, M. I.; Anderson, M. A. *Langmuir* **1997**, *13*, 4829.
- (35) Takeuchi, M.; Martra, G.; Coluccia, S.; Anpo, M. *J. Phys. Chem. B* **2005**, *109*, 7387.
- (36) Shepot'ko, M. L.; Davydov, A. A. *Theor. Exp. Chem.* **1991**, *27*, 232.
- (37) Glisenti, A. *J. Mol. Catal. A: Chem.* **2000**, *153*, 169.
- (38) Zhuravlev, L. T. *Colloids Surf., A* **2000**, *173*, 1.